Chapter 14
Focused Ion Beam-Assisted Nanoscale Processing and Thermoelectrical Characterization

Kyung-Min Lee and Tae-Youl Choi

Abstract In this report, we introduce a nanomanipulation and fabrication technology, which is useful to characterize thermoelectrical properties of individual one-dimensional nanosystems such as metallic or semiconducting carbon nanotubes (CNTs) and nanowires (NWs). For such characterization, a one-stop measurement platform was constructed by focused ion beam (FIB) nanolithography after which a freestanding NW was picked up from a bundle of NWs and placed on the platform using a nanomanipulator. As a unique and unparalleled control for nanoscale one-dimensional systems, FIB-assisted nanomanipulator could make a direct access to nanoscale materials and structures. Subsequently, the four-point 3-ω method combined with a nanoheater was used to obtain electrical conductivity, thermal conductivity, and Seebeck coefficient, with which one can estimate the figure of merit of β-silicon carbide (SiC) NWs. We found that the thermal conductivity of a single β-SiC NW was 82 ± 6 W/mK. The Seebeck coefficient was also successfully measured to be -1.21 mV/K. With a measured electrical conductivity of the NW, the dimensionless thermoelectrical figure of merit (ZT) was estimated to be 0.12.

14.1 Introduction

As a unique and unparalleled manipulation, fabrication, and characterization tool, focused ion beam (FIB) has played an important role in nanotechnology because of its site-specific working range up to a few nanometers and direct and straightforward access to a nanoscale structure. The first commercial instrument was

K.-M. Lee • T.-Y. Choi (✉)
Department of Mechanical and Energy Engineering, University of North Texas, Denton, TX 76203-1098, USA
e-mail: KyungminLee@my.unt.edu; choi@egw.unt.edu

Z.M. Wang (ed.), *FIB Nanostructures*, Lecture Notes in Nanoscale Science and Technology 20, DOI 10.1007/978-3-319-02874-3_14,

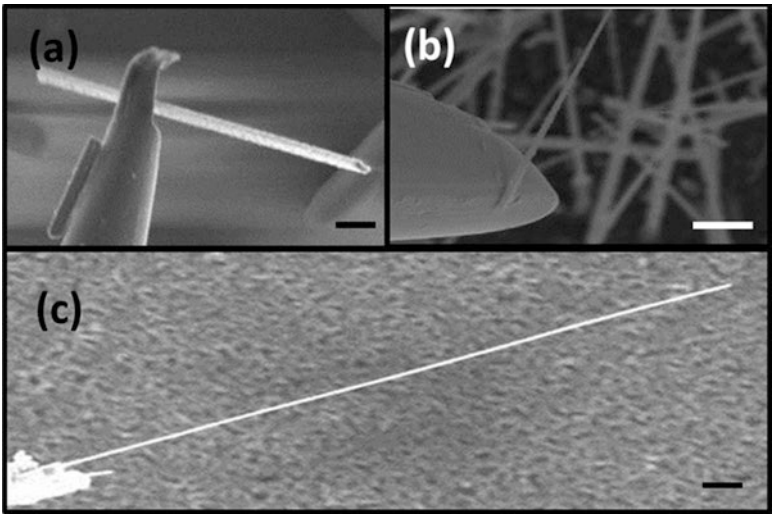

Fig. 14.1 Direct manipulation of various NWs with a nanomanipulator annexed to FIB. (**a**) Ag NW attached to a nanomanipulator; (**b**) a single Si NW extracted from a bundle of Si NW by a nanomanipulator; (**c**) a β-SiC NW attached to a nanomanipulator. Each scale bar in the images indicates 1 μm

introduced in the market more than decades ago [1] since the prototype dual-beam technique was developed during the late 1970s and the early 1980s.

As liquid-metal ion sources (LMISs) are most commonly used, a gallium ion source was adopted in our study. A heated, thus liquid molten metal in contact with a tungsten needle wets the tungsten, and an electric field greater than 10^8 V/cm initiates ionization and field emission of the gallium ions. Then the emitted ions are accelerated to energy of 5–50 keV and focused onto the sample through electrostatic lenses. Working at such small scale, FIB is able to modify tiny circuits and small surface areas and to deposit and etch materials with chemical reactions of Ga^+ ions (which are ejected from an FIB column) and reactants. FIB is now broadly used in various technological fields such as semiconductor and nanotechnology. FIB employs a nanomanipulator (attached to FIB), which has played and plays an important role to manipulate nanostructures such as picking (lifting) up and placing FIB-fabricated nano- and microstructures for transmission electron microscope (TEM) sample preparation. The nanomanipulator whose tip end is at a submicron size is small enough to control nanostructures such as NWs. Figure 14.1 shows various previous results of manipulated NWs (β-SiC, silicon (Si), and silver (Ag) NWs). This way, direct access to such a tiny structure with a finely focused ion beam and manipulator has made FIB to be a powerful and necessitated tool to work in the area of nanotechnology. Also, the relevant technologies such as fine arts of machining, drawing, and structuring have been much emphasized as more demands on well-defined nanostructures arise. This motivated us in the research to employ the FIB technology to characterize the thermoelectrical properties of NWs [2–4].

We used an Omniprobe (AutoProbe™ 200) nanomanipulator attached to a dual-beam FIB machine that enables fine control of nanostructures, e.g., creating mechanical repositioning of NWs. The nanomanipulator used in our study has 100 nm positioning resolution. It has been served as a fully automated and multipurpose nano-positioning tool that is able to make in situ lift-out, electrical measurements, nano-mechanical testing, and charge neutralization in FIB and SEM [5]. FIB used in our study was FEI Nova 200 NanoLab, which has been operated since January 2005 in the Center for Advanced Research and Technology (CART) at UNT. The secondary electron image resolution is 1.5 nm at 15 kV. The focused ion beam has better than 7 nm resolution at 30 kV.

In this article, we report thermoelectrical characterization of a single β-SiC NW. Being a material possessing superior physical properties such as high thermal conductivity, high mechanical strength, and wide bandgap structure, SiC has been used as a substantial material for applications in microelectronic, thermoelectric, and optoelectronic devices [6–9]. Mostly, the material has been used in a harsh environment such as high power, high frequency, and high temperature because of its physical and chemical durability and stability. Thus, it has a potential to replace Si in the near future. Owing to its excellent physical properties, this one-dimensional NW structure has been greatly interesting for scientific and technological research. Following this trend, SiC NWs have attracted much attention because of the excellent low-dimensional feature as well as their aforementioned intrinsic properties. For this reason, SiC NWs have been considered as important electric devices such as field-effect transistors (FETs) [10–12]. SiC crystallizes in more than 200 polytypes but the variants that have received the most research attention are the β-SiC (3C-SiC) zincblende form (studied in this article) and the 6H-, 4H-, hexagonal polymorphs.

14.2 Nanofabrication of One-Stop Measurement Platform

14.2.1 Focused Ion Beam Milling Process

FIB can locally etch and mill a sample surface with nanoscale precision. The sputtering rate of a sample in FIB milling is affected by various parameters explained below and material properties as in other sputtering systems. The beam current, sample density, sample atomic mass, and incoming ion mass are factors to affect the FIB milling. The removal of a sample material is achieved by an energetic Ga+ beam that is used in our FIB. The result is physical sputtering of the sample material, as illustrated schematically in Fig. 14.2. By scanning the focused Ga+ beam over the substrate, a predefined shape can be obtained through milling and etching the surface of the substrate.

For the thermal conductivity measurement based on the 3-ω method, a prepatterned metal electrode structure was made by standard photolithography

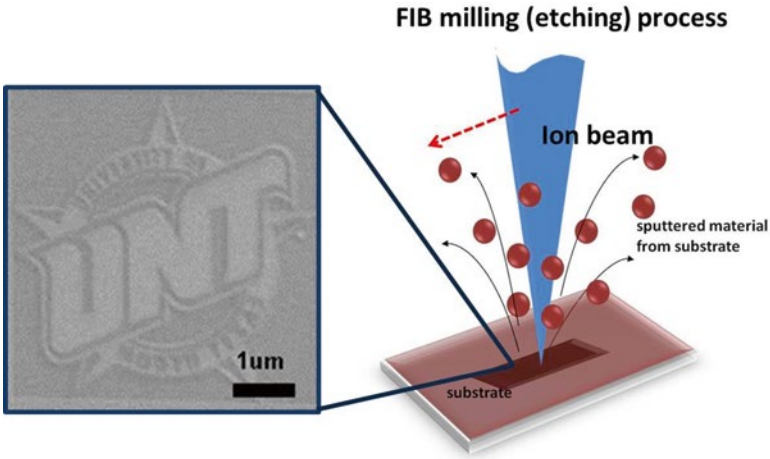

Fig. 14.2 Schematic FIB milling process and UNT logo created by FIB milling (CART at UNT acknowledged for its permission to reproduce the UNT logo)

processes. Then, FIB was utilized to create a fine nanoscale structure consisting of four-point contact probes by milling. Figure 14.3 shows the process of fabricating the four-point probe structure for the 3-ω thermal conductivity method.

A silicon nitride (Si_3N_4) membrane with 500 nm thickness that had been grown on a Si wafer was used as a substrate in this study. Potassium hydroxide (KOH) was used for selectively etching Si at the center of the substrate to create a thin membrane structure with dimension of 300×300 μm^2. A microelectrode pattern was created by sputtering deposition of Au/Cr on top of the membrane. The standard photolithography technique was employed to pattern electrodes for an electrical interface. The reason for creating the membrane structure is to make a through hole that serves as thermal insulation in the thermal conductivity and Seebeck coefficient measurement. This hole can prevent heat generated at the NW due to Joule heating from leaking through the substrate. The trench and four-point probe structures were created with an aid of FIB milling.

On the pre-patterned electrode, a focused ion beam of 30 kV (at 0.1 nA current and at 5,000 magnification) was applied for shaping a four-point probe structure. In situ observation with SEM was made to determine when to stop the milling process. This helped us save the processing time and avoid undesired damages on electrodes. The trench was created sequentially with the same ion beam intensity. At this time, we carefully observed the beam current change on a controlling panel in an FIB operation software instead of direct monitoring of the milling process with in situ SEM observation. This allowed us to create a well-defined and finely tailored trench with minimal damage of adjacent electrodes. We believe that in situ SEM observation can induce ion beam distortion and drift as a result of ion and electron beam interaction; thus, it is suitable for relatively large-scale milling.

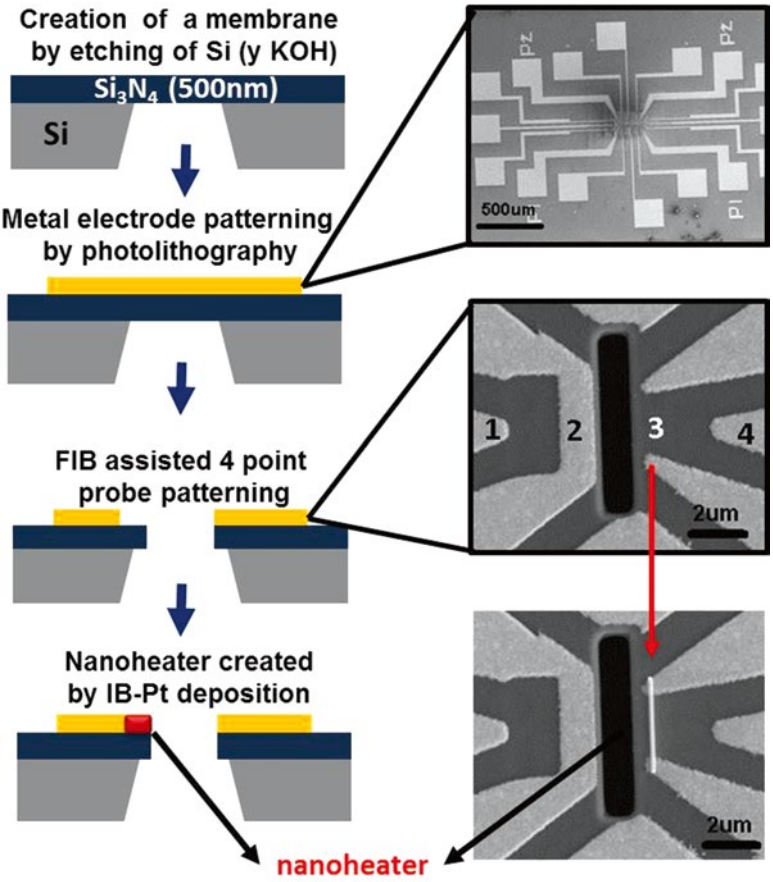

Fig. 14.3 Fabrication of four-point probe platform for the 3-ω thermal conductivity measurement

14.2.2 Focused Ion Beam Deposition Process

Technological advancement in making nanoscale devices is nowadays more demanded as novel and superior physical phenomena in the nanostructure have been discovered. In particular, excellent thermal transport characteristics in nanoscale devices have been revealed and thus attracted a particular interest because of its potential in thermal management applications. Herein, we introduce a new way of inducing nanoscale heating to create a highly localized heat source. This allowed us to successfully measure Seebeck coefficient (hence thermoelectric figure of merit) through accurate temperature calibration of the heater and measurement of temperature across the suspended SiC NW [13].

In Fig. 14.3, the number 3 probe was coated with an ion beam-induced platinum (IB-Pt) thin stripe for measuring the Seebeck coefficient. The IB-Pt stripe was

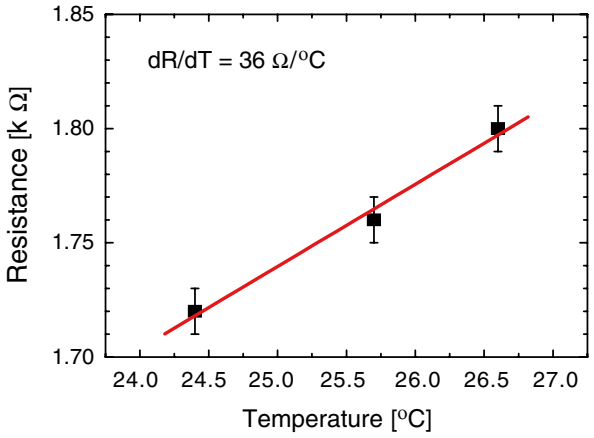

Fig. 14.4 The resistance change by temperature variation of the nanoheater created by IB-Pt deposition. It shows that the resistance change by temperature variation of the nanoheater is 36 Ω/°C (reproduced from [15], ©Nano Science and Technology Institute)

manufactured by FIB deposition process at 30 kV/10 pA intensity for a finely defined structure. Because there should be a localized heat source to a NW for Seebeck coefficient measurement (for temperature gradient), the IB-Pt thin stripe was found to be a better heating source than the thin stripe of Au because higher resistance (~1.7 kΩ) could be achieved across the IB-Pt heater stripe. This high resistance is needed to accurately calibrate the nanoheater (resistance vs. temperature); the change of lead resistance of Au electrodes during calibration will be ignored. This type of nanoheater can also increase the sensitivity of temperature measurement due to the high temperature coefficient. The high resistance is attributed to an intrinsic electrical property of IB-Pt as it contains a higher amount of carbon that makes IB-Pt highly resistive to electrical conduction than a pure metal; the literature value of resistivity of IB-Pt is 10–20 μΩm depending on deposition condition [14].

The coated IB-Pt thin line (i.e., nanoheater) had a dimension of $200 \times 100 \times 2{,}300\ \text{nm}^3$. One of the strengths of this structure is that its resistance can be easily controlled by its geometrical configuration. We have tested the resistance change of the IB-Pt thin line due to the change of its geometry and obtained 17 kΩ for a nanoheater with a size of 200 nm × 100 nm × 25 μm. If it was scaled down to 2.3 μm which is the same length of the nanoheater shown in Fig. 14.3, the resistance could be 1.56 kΩ. This value was close to the measured value of the nanoheater that was used for Seebeck coefficient characterization. Therefore, it was concluded that the IB-Pt deposition process could control the resistance of the nanoheater by defining its geometry. The resistance of one particular nanoheater fabricated by FIB deposition process was 1.72 kΩ at room temperature which was a good localized heating source for accurate measurement of Seebeck coefficient. Figure 14.4 shows a calibration curve which is the result of resistance change by temperature variation of the nanoheater. We fabricated various nanoheaters with specific resistance values. One of them was used to measure the Seebeck coefficient of a single β-SiC NW. Figure 14.5 shows three nanoheaters with different thickness and width created by IB-Pt deposition.

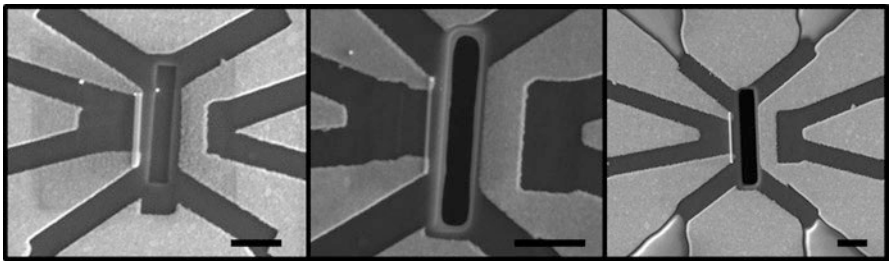

Fig. 14.5 IB-Pt thin lines (nanoheaters) whose lengths were ~2 μm and diameters were a few hundred nanometers. Each bar in the images is 2 μm long

14.2.3 Control of Nanomaterials Using a Nanomanipulator

Controlling NWs is one of the most challenging tasks, and still novel methods are being developed including the methods assisted by molecular, electrostatic, and shear forces [16–18]. Another well-known method is to use nonuniform electric field and polarizability of NW to place a single NW on a desired location. The so-called dielectrophoresis (DEP) uses a phenomenon that a polarizable material tends to move in a converging electrical field [19–22]. Methods employing DEP are required to have specifically designed electrodes (to create nonuniform electric field) and optimization of applied field strength and frequency. Due to the geometrical constraints in the configuration of the four-point probe electrodes, it was revealed that DEP was not appropriate for our work, resulting in a low yield (less than 10 % success). Another concern is on the cleaning after using the DEP method for NW control, where NW-dissolved solution should be dropped on the measurement platform before applying the electric field. The force created by the applied field attracted not only NWs but also other particles and dust inside of a droplet of NW solution. Careful cleaning and rinsing residues and contaminants in the measurement platform should be unavoidable.

In order to overcome drawbacks in the DEP method, we used a direct approach to place a single NW on the measurement platform using a nanomanipulator. We used the van der Waals interaction between a nanomanipulator and an NW when a submicron-sized tip of a nanomanipulator approaches a single NW within a range of molecular force being effective. Before a nanomanipulator touches the NW, for clear viewing and easy controlling, the tip end of the nanomanipulator was sharpened by a high-intensity FIB at 30 kV/1 nA. Once the nanomanipulator contacted a NW, an electron beam-induced Pt (EB-Pt) deposition was made between the nanomanipulator and the NW for secure adhesion by using focused electron beam (5 kV/98 pA e-beam intensity). Then, we could obtain a single NW by withdrawing the nanomanipulator with high acceleration. Omniprobe (AutoProbe™ 200) nanomanipulator (Omniprobe, Inc.) attached to the FIB machine (FEI Nova 200 NanoLab) was employed for this technique, and a motion control system of the nanomanipulator was extremely accurate and repeatable within 100 nm of stage

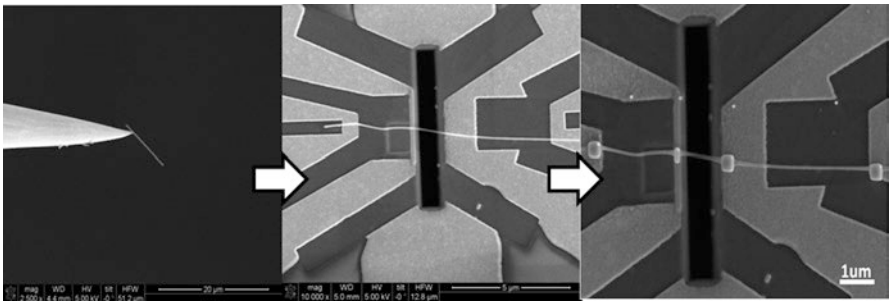

Fig. 14.6 A single β-SiC NW was obtained from a host of bundles or substrates using the nanomanipulator and placed on the four-point probe measurement platform. At the last step, the contact points with the probe were covered with EB-Pt deposition

displacement over the entire range of motion. Figure 14.6 shows SEM images of a single NW obtained and placed on the four-point probe measurement platform by the nanomanipulation technique in series of steps. This direct manipulation technique was also applied to obtain specific NWs of the same material to compare their geometrical influences to thermal conductivities [23].

The four contact points between the NW and the probe electrodes were fully covered by EB-Pt deposition. This allowed for the reduction of the contact resistance between the NW and the electrode at each contact point. After the EB-Pt deposition on the contact points, the NW sample was annealed at 400 °C under high vacuum (10^{-6} Torr) to further minimize the electrical contact resistance. It has been reported that the annealing step could remove the voids in the contact points between the NW and probe electrodes [24].

14.3 Electrical and Thermal Conductivity

The one-stop measurement setup is depicted in Fig. 14.7. Electrical and thermal conductivities and Seebeck coefficient could be measured in this one-stop measurement platform in situ. The measurement platform consists of the four-point probe and nanoheater. A lock-in amplifier (Stanford Research System SR850) was connected to the measurement system to read 3-ω signals for thermal conductivity measurement. An alternating current (AC) source (Keithley 6221) was used for a stable current supply. In addition to providing a stable current, the compliance setting of the current source could prevent any undesirable overshooting as any unwanted high current density might damage the placed NW.

In order to measure the thermal conductivities of individual NWs, microfabrication-assisted device structures have been suggested [25–29]. We used the 3-ω method in this study. The 3-ω method is based on a four-point probe system, which enables measurements of magnitude and phase of third-harmonic signal for one-dimensional sample subject to AC modulated at the fundamental frequency of ω. As a

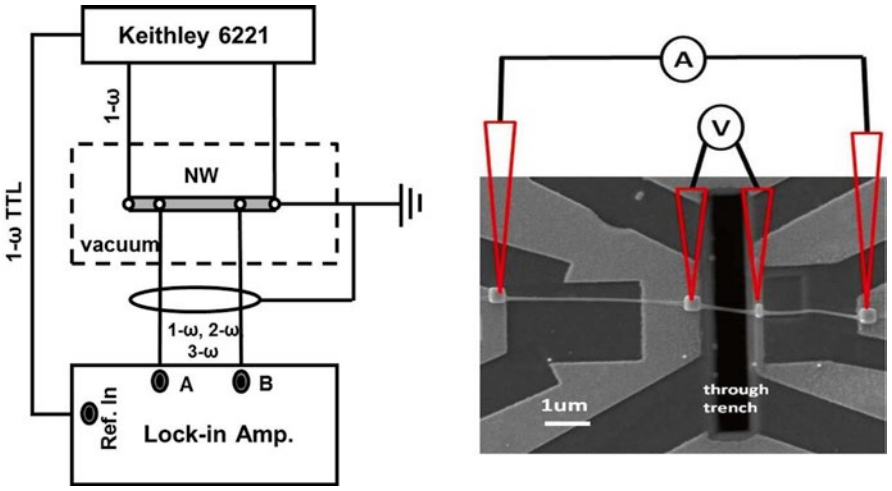

Fig. 14.7 Four-point probe measurement setup for electrical and thermal conductivities and Seebeck coefficient (reproduced from [13], ©Springer)

time-independent frequency-domain technique, the 3-ω method can effectively eliminate spurious signals because a narrow-band detection technique is employed. This in turn enhances signal-to-noise ratio which allows for more accurate signal reading. Thus, the 3-ω method has been employed in various fundamental thermal characterizations including measurement of thermal conductivity for CNTs and bulk structure [30–32]. The third-harmonic amplitude created as a response to an applied AC current with a fundamental frequency has information about the 1D sample's thermal conductivity as shown in the following equation [31, 33]:

$$V_{3\omega,rms,vac} \cong \frac{\sqrt{2}I_0^3 RR'L}{\pi^4 kA} \tag{14.1}$$

where L, $R[=R_0+R'(T-T_0)]$, and A are length, electrical resistance, and cross-sectional area of NW, respectively. R' is the temperature coefficient of resistance at room temperature defined as $(dR/dT)_{\text{room temp.}}$ and k is the thermal conductivity of NW. The advantage of this method can minimize the uncertainty due to the contact resistance which is present in the conventional two-point probing method.

The electrical resistivity of the β-SiC NW was measured to be $\sim 4.45 \times 10^{-3}$ Ωcm from the first-harmonic AC signal (1 kHz) and geometry of the NW (diameter of 60 nm and length of 1.5 μm). From the measured third-harmonic signals, we have estimated the thermal conductivity to be 82 ± 6 W/mK. The third-harmonic signals as a function of AC current amplitude at 1 kHz detected by the lock-in amplifier are shown in Fig. 14.8a. The data were best-fitted according to (14.1) and the result of the matching exponent of 2.83 was obtained. This value was very close to the theoretical value of 3.

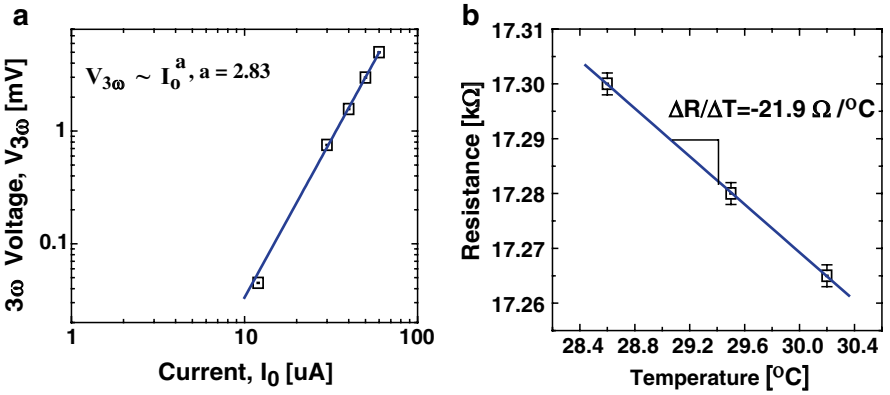

Fig. 14.8 (**a**) 3-ω voltage signals as a function of current, I_0, obtained at room temperature; (**b**) the resistance change by temperature gradient of a single β-SiC NW (reproduced from [13], ©Springer)

In order to obtain the thermal conductivity of NW by the 3-ω method, the temperature coefficient (resistance change by temperature variation) should be known according to (14.1). In the temperature range of 28.6–30.2 °C, the resistance change by temperature variation was measured at −21.9 Ω/°C (Fig. 14.8b). The negative sign is verified by the fact that SiC nanowire is semiconducting.

14.4 Seebeck Coefficient and Figure of Merit

Seebeck coefficient, S, was measured immediately after characterizing the thermal conductivity. For a semiconductor, Seebeck coefficient can be written as [13]

$$S = -\frac{k_B}{e}\left(\frac{E_F - E_c}{k_B T} + const.\right) \cong \frac{\left(E_c - E_F\right)}{eT} \tag{14.2}$$

where E_c is the conduction band energy, E_F is the Fermi energy, e is the electron charge, k_B is the Boltzmann constant, and T is the temperature. As seen in (14.2), Seebeck coefficient can be maximized when E_F is located inside the bandgap. However, lowering E_F to increase the gap induces reducing electrical conductivity. This will have the adverse effect on the thermoelectric figure of merit, which can be written as $Z\ (=S^2\sigma/\kappa)$ where σ is the electrical conductivity and κ is the thermal conductivity. Therefore, in an n-type semiconductor such as β-SiC NW, the optimal condition for a large value of Seebeck coefficient is that Fermi level should be close to the band edge without lowering an electrical conductivity. In this study, Seebeck coefficient was obtained from a voltage change by a thermal gradient across the NW such as $S = -(dV/dT) = -(\Delta V/\Delta T)$. The thermal gradient was established by a localized heating source created by IB-Pt. The localized heating source (nanoheater) was

made of a thin line through IB-Pt deposition. The calibration for the resistance change by temperature change of the nanoheater was conducted to find an actual temperature of the heater when an electrical current is applied. Keithley 6221 AC/DC current source and Keithley 2182A nanovoltmeter were used to find the resistance change of the heater as the temperature increases. An electrical power from a power supply was provided to an aluminum (Al) block through the cartridge heater. A temperature sensor was used to read the temperature of the sample and Al block when an electric power was given to the cartridge heater. A high-speed A/D (analog-digital) converter (AD7760) was used to transfer and control analog signals such as power and temperature via LabVIEW® program in a computer. The data flows between a computer and A/D converter were made through a serial (e.g., USB) interface.

The measured value of resistance change by temperature gradient of the nanoheater was revealed to be 36 Ω/°C. From the calibrated value of resistance change by temperature gradient of the nanoheater, we could determine the temperature vs. applied current. Once the temperature of the nanoheater was known, the voltage drop was measured between the two inner probes out of the four-point probes. This revealed the voltage change by temperature gradient between the two inner probes (i.e., the nanoheater and the probe across the trench). Voltage and temperature difference, ΔV and ΔT, were measured to be 2.015×10^{-3} V and 1.67 °C. Thus, the Seebeck coefficient of the placed NW was −1.21 mV/K from the definition, $S = -(\mathrm{d}V/\mathrm{d}T) = -(\Delta V/\Delta T)$. Finally, the dimensionless thermoelectric figure of merit, ZT ($=S^2\sigma T/\kappa$), was estimated to be 0.12 from all the measured values of σ, κ, and S at room temperature.

14.5 Conclusions

For measurement of thermal properties of a single NW, we developed a one-stop measurement platform consisted of four-point probes and nanoheater. Combining FIB and nanomanipulator, we placed a freestanding single NW (i.e., β-SiC NW) on the specific location of the measurement platform. Subsequently, its thermoelectrical properties such as electrical and thermal conductivities and Seebeck coefficient were measured. From the obtained data, the dimensionless thermoelectric figure of merit was also estimated. This FIB-assisted nanoscale processing would allow us to make more accurate thermoelectrical measurements of nanostructures such as NW and nanotube and to have better fundamental understanding of their thermal behaviors.

References

1. Melngailis, J.: Critical review: focused ion beam technology and applications. J. Vac. Sci. Technol. B **5**, 469 (1987)
2. Reyntjens, S., Puers, R.: A review of focused ion beam applications in microsystem technology. J. Micromech. Microeng. **11**, 287 (2001)

3. Reyntjens, S., De Bruyker, D., Puers, R.: Focused ion beam as an inspection tool for microsystem technology. Proceedings of the 1998 Microsystem Symposium, vol. 125, Delft, the Netherlands (1998)
4. Ward, B.W., Economou, N.P., Shaver, D.C., Ivory, J.E., Ward, M.L., Stern, L.A.: Microcircuit modification using focused ion beams. Proc. SPIE **923**, 92 (1988)
5. Orloff, J., Utlaut, M., Swanson, L.: High resolution focused ion beams: FIB and its applications. Springer Press, New York (2003)
6. Casady, J.B., Johnson, R.W.: Status of silicon carbide (SiC) as a wide-bandgap semiconductor for high-temperature applications: a review. Solid-State Electron. **39**, 1409 (1996)
7. Wong, E.W., Sheehan, P.E., Lieber, C.M.: Nanobeam mechanics: elasticity, strength, and toughness of nanorods and nanotubes. Science **277**, 1971 (1997)
8. Liang, C.H., Meng, G.W., Zhang, L.D., Wu, Y.C., Cui, Z.: Large-scale synthesis of b-SiC nanowires by using mesoporous silica embedded with Fe nanoparticles. Chem. Phys. Lett. **329**, 323 (2000)
9. Shenai, K., Scott, R.S., Baliga, B.J.: Optimum semiconductors for high-power electronics. IEEE Trans. Elec. Dev. **36**, 1811–1823 (1989)
10. Dai, H.J., Wong, E.W., Lu, Y.Z., Fan, S.S., Lieber, C.M.: Synthesis and characterization of carbide nanorods. Nature (London) **375**, 769 (1995)
11. Li, Z.J., Li, H.J., Chen, X.L., Meng, A.L., Li, K.Z., Xu, Y.P., Dai, L.: Large-scale synthesis of crystalline β-SiC nanowires. Appl. Phys. A Mater. Sci. Process **76**, 637 (2003)
12. Rogdakis, K., Lee, S.Y., Bescond, M., Lee, S.K., Bano, E., Zekentes, K.: Theoretical comparison of 3C-SiC and Si nanowire FETs in ballistic and diffusive regimes. IEEE Trans. Elec. Dev. **55**, 1970–1976 (2008)
13. Lee, K.M., Lee, S.K., Choi, T.Y.: Highly enhanced thermoelectric figure of merit of a β-SiC nanowire with a nanoelectromechanical measurement approach. Appl. Phys. A **106**, 955–960 (2012)
14. Platinum deposition Technical note (FEI Company, Hillsboro, OR) PN 4035 272 21851-D (2003)
15. Lee, K.M., Choi, T.Y., Lee, S.K.: Measurement of figure of merit for a singleβ-silicon carbide nanowire by the four-point three-ω method. TechConnect World 2010 Proceedings (Nanotechnology 2010) vol. 2, pp. 202–205 (2010)
16. Lee, J., Wang, A.A., Rheem, Y., Yoo, B., Mulchandani, A., Chen, W., Myung, N.V.: DNA assisted assembly of multisegmented nanowires. Electroanalysis **19**(22), 2287 (2007)
17. Heo, K., Cho, E., Yang, J.E., Kim, M.H., Lee, M., Lee, B.Y., Kwon, S.G., Lee, M.S., Jo, M.H., Choi, H.J., Hyeon, T., Hong, S.: Large-scale assembly of silicon nanowire network-based devices using conventional microfabrication facilities. Nano Lett. **8**(12), 4523 (2008)
18. Deegan, R.D., Bakajin, O., Dupont, T.F., Huber, G., Nagel, S.R., Witten, T.A.: Contact line deposits in an evaporating drop. Phys. Rev. E **62**(1), 756 (2000)
19. Liu, Y., Chung, J., Liu, W.K., Ruoff, R.S.: Dielectrophoretic assembly of nanowire. J. Phys. Chem. B **110**, 14098–14106 (2006)
20. Chung, J., Lee, K., Lee, J., Ruoff, R.S.: Toward large-scale integration of carbon. Nanotubes (Langmuir) **20**(8), 3011–3017 (2004)
21. Boote, J.J., Evans, S.D.: Dielectrophoretic manipulation and electrical characterization of gold nanowires. Nanotechnology **16**, 1500–1505 (2005)
22. Schwamb, T., Choi, T.Y., Schirmer, N., Bieri, N.R., Burg, B., Tharian, J., Sennhauser, U., Poulikakos, D.: Dielectrophoretic method for high yield deposition of suspended, individual carbon nanotubes with 4-point electrode contact. Nano Lett. **7**, 3633 (2007)
23. Lee, K.M., Choi, T.Y., Lee, S.K., Poulikakos, D.: Focused ion beam-assisted manipulation of single and double β-SiC nanowires and their thermal conductivity measurements by the four-point-probe 3-ω method. Nanotechnology **21**, 125301 (2010)
24. Gopal, V., Radmilovic, V.R., Daraio, C., Jin, S., Yang, P., Stach, E.A.: Rapid prototyping of site-specific nanocontacts by electron and ion beam assisted direct-write nanolithography. Nano Lett. **4**, 2059 (2004)

25. Shi, L., Hao, Q., Yu, C., Mingo, N., Kong, X., Wang, Z.L.: Thermal conductivities of individual tin dioxide nanobelts. Appl. Phys. Lett. **84**, 2638 (2004)
26. Li, D., Wu, Y., Kim, P., Shi, L., Yang, P., Majumdar, A.: Thermal conductivity of individual silicon nanowires. Appl. Phys. Lett. **83**, 2934 (2003)
27. Wang, J., Wang, J.-S.: Carbon nanotube thermal transport: ballistic to diffusive. Appl. Phys. Lett. **88**, 111909 (2006)
28. Bryning, M.B., Milkie, D.E., Islam, M.F., Kikkawa, J.M., Yodh, A.G.: Thermal conductivity and interfacial resistance in single-wall carbon nanotube epoxy composites. Appl. Phys. Lett. **87**, 161909 (2005)
29. Vavro, J., Llaguno, M.C., Satishkumar, B.C., Luzzi, D.E., Fischer, J.E.: Electrical and thermal properties of C_{60}-filled single-wall carbon nanotubes. Appl. Phys. Lett. **80**, 1450 (2002)
30. Choi, T.Y., Poulikakos, D., Tharian, J., Sennhauser, U.: Measurement of thermal conductivity of individual multiwalled carbon nanotubes by the 3-ω method. Appl. Phys. Lett. **87**, 013108 (2005)
31. Choi, T.Y., Poulikakos, D., Tharian, J., Sennhauser, U.: Measurement of the thermal conductivity of individual carbon nanotubes by the four-point three-ω method. Nano Lett. **6**, 1589 (2006)
32. Lu, L., Yi, W., Zhang, D.L.: 3ω method for specific heat and thermal conductivity measurements. Rev. Sci. Instrum. **72**, 2996 (2001)
33. Yi, W., Lu, L., Dian-lin, Z., Pan, Z.W., Xie, S.X.: Linear specific heat of carbon nanotubes. Phys. Rev. B **59**, R9015 (1999)